Magnetic dead layer at the interface between a Co film and the topological insulator Bi_{2}Se_{3}

J. Li, Z. Y. Wang, A. Tan, P.-A. Glans, E. Arenholz, C. Hwang, J. Shi, and Z. Q. Qiu

Phys. Rev. B **86**, 054430 — Published 20 August 2012

DOI: 10.1103/PhysRevB.86.054430

Magnetic dead layer at the interface between Co film and topological insulator Bi_2Se_3

J. Li,[1] Z. Y. Wang[2], A. Tan,[1] P.-A. Glans,[3] E. Arenholz,[3] C. Hwang,[4] J. Shi,[2] and Z. Q. Qiu[1]

[1] Department of Physics, University of California at Berkeley, Berkeley, California 94720, USA

[2] Department of Physics, University of California at Riverside, Riverside, California 94521, USA

[3] Advanced Light Source, Lawrence Berkeley National Laboratory, Berkeley, California 94720, USA

[4] Korea Research Institute of Standards and Science, Yuseong, Daejeon 305-340, Republic of Korea

Abstract

Co films were grown on top of topological insulator Bi_2Se_3(111) substrate and studied using Magneto-Optic Kerr Effect (MOKE) and X-ray Magnetic Circular Dichroism (XMCD). Both MOKE and XMCD results show that there exists a ~1.2nm thick magnetic dead layer of the Co film, i.e., ~1.2nm Co film at the Co/Bi_2Se_3(111) interface losses its ferromagnetic order. The Co ferromagnetic order can be completely resumed by inserting a 3 nm Ag layer between the Co and Bi_2Se_3, indicating that the magnetic dead layer is due to the Co/Bi_2Se_3 interfacial mixing which is supported by the Co L edge spectroscopy result.

PACS numbers: 75.70.Ak, 68.43.Bc, 68.37.Ef, 68.43.Jk

1. Introduction

Topological insulators (TIs) merge as a new class of insulators on which there exists a topologically protected state at the boundary of the insulator [1,2,3,4,5]. Both two-dimensional and three-dimensional TIs were soon discovered after the theoretical predictions [6,7], and have generated a great research activity in condensed matter physics [8,9]. One unique property of the topological surface state is that the massless Dirac state has the electron spin direction locked perpendicular to its momentum so that electrons with opposite momenta have opposite spin directions, leading to a diminishment of the electron backscattering [10,11]. In contrast, time-reversal symmetry breaking (e.g., by magnetic field or magnetic impurities) is expected to open an energy gap and suppresses the local density of states [12]. This makes TIs an important candidate for spintronics applications. For example, large Magneto-Optic Effect is predicted in TIs [13] and was indeed confirmed by Terahertz Magneto-Optic Kerr Effect (MOKE) measurement [14]. Crossover between weak antilocalization and localization is also observed in magnetically doped TIs [15,16]. While applying a magnetic field to break the time-reversal symmetry yields a clean result [14,16], adding magnetic elements to a TI yields somewhat ambiguous results. For magnetically doped TIs, both angle resolved photoemission spectroscopy (ARPES) [17] and scanning tunneling microscopy (STM) [18] clearly reveal time-reversal symmetry breaking features such as the gap opening at the Dirac point. Direct magnetic measurement on magnetically doped TIs also shows a Curie-like behavior although the derived magnetic ordering temperature is only ~10K [19]. The low ordering temperature can be enhanced to near room temperature by the deposition of a ferromagnetic (FM) layer on top of the magnetically doped TI, indicating that the surface state in magnetically doped TIs already acquired magnetic characters so that it can be polarized by the proximity effect from the FM overlayer [20]. For direct deposition of magnetic element on top of TIs, however, the experiments show controversial result. An ARPES work by AndrewWray et. al shows an energy gap opening at the Dirac point upon deposition of Fe on Bi_2Se_3 [21]. However, another ARPES work shows that there is no any difference around the Dirac point between magnetic and nonmagnetic adsorbates, questioning previous claim of the magnetic induced gap [22]. A STM study for Fe deposited on TIs showed different spectroscopy characters at different temperatures above the Fe atoms, suggesting possible different occupation sites of the Fe atoms on top of the TI [23]. Another experiment on the other hand shows that although the deposited Fe atoms could develop magnetic moments, the Fe absorbates won't

open an energy gap at the Dirac point [24]. A recent STM/ARPES combined experiment further shows the absence of both the FM order and the energy gap opening for submonolayer Co absorbates on Bi_2Se_3 although it is unclear if a Co film thicker than 0.45ML would yield the FM order at the interface [25]. Recent theoretical calculation also suggests that the surface state of a TI could survive upon magnetic Mn doping [26]. The above controversial results raise a critical issue that if a deposited FM layer on top of a TI is FM ordered at the FM/TI interface? Since many theoretical proposals related to spintronics in FM/TI system crucially depend on the FM interfacial state such as the spin dynamics of the FM overlayer [27,28], ordered-to-spinglass magnetic phase transition [29], and the spin current injection [30,31], etc, it is very important to clarify in experiment if the FM layer in a FM/TI system is FM ordered at the interface? In this paper, we report a detailed thickness-dependent study of Co film grown on Bi_2Se_3. Using both Magneto-Optic Kerr Effect (MOKE) and element-specific X-ray Magnetic Circular Dichroism (XMCD) measurements, we show that the Co layer on top of Bi_2Se_3 is not FM ordered at the interface. By inserting a Ag spacer layer between Co and Bi_2Se_3, the Co at the Co/Ag interface resumes the FM order.

2. Experiment

A multi-step heating procedure was employed for Bi_2Se_3 single crystal growth. Small pieces of high-purity (99.999%) Bi_2Se_3 compound were put in a quartz tube which was evacuated and sealed. The tube was heated up to and kept at 400°C for 16 hours in a programmable furnace. The temperature was then ramped to 800°C and kept for 24 hours. After that it was slowly cooled down to 550°C in one day and kept at this temperature for three more days before cooling down to room temperature. The Bi_2Se_3(111) crystal was cleaved in an ultrahigh vacuum (UHV) system of a base pressure of 2×10^{-10} Torr. The size of the cleaved Bi_2Se_3 substrate is ~5mm in diameter. Low Energy Electron Diffraction (LEED) confirms the Bi_2Se_3(111) single crystalline surface after the cleavage [Fig. 1(a)]. Co film is grown on top of the Bi_2Se_3 substrate by evaporating Co from an e-beam evaporator. The evaporation rate was monitored by a quartz thickness monitor which was calibrated by Reflection High Energy Electron Diffraction (RHEED) oscillations [32]. LEED result shows that the Co forms polycrystalline film on top of the Bi_2Se_3(111) substrate [Fig. 1(b)]. For thickness-dependent study, Co wedges were grown by moving

the substrate behind a knife-edge shutter. The wedge has a thickness range of 0-2.5nm over 2mm distance.

3. Result and Discussion

To have a systematic thickness-dependent study, the sample was measured *in situ* using Magneto-Optic Kerr Effect (MOKE) during the sample growth. For MOKE measurement, a linearly p-polarized HeNe laser serves as the light source. After reflection from the sample surface, the light intensity is detected by a photodiode with a linear (analyzing) polarizer in front of it. The analyzing polarizer is set at a small angle (δ~2^o) from the extinction condition to provide a d.c. bias. Then the reflected intensity (I) as a function of the external magnetic field (B) measures the magnetic hysteresis loop of the Co film with the reflection intensity (I) related to the Kerr rotation (ϕ_K) by $I = I_0\left(1+\frac{2\phi_K}{\delta}\right)$ or $\phi_K = \frac{\delta}{4}\cdot\frac{I_+ - I_-}{I_0}$, where $I_0 = (I_+ + I_-)/2$ is the d.c. biased reflection intensity and I_+ and I_+ are the reflection intensity for $+B$ and $-B$, respectively [33]. Because of the birefringence of the UHV viewport, a quarter waveplate was actually used in front of the analyzing polarizer so that the measured quantity is Kerr ellipticity (imaginary part of the Kerr complex rotation) [33]. Throughout the Co thickness range, we only observed longitudinal Kerr signal (magnetic field in the plane of the film) so that the easy magnetization axis of the Co/Bi_2Se_3 is in the film plane, the same as Fe/TI [24]. Representative hysteresis loops of the Co/Bi_2Se_3 are shown in Fig. 2(a). FM hysteresis loop is observed only above ~1.2nm Co thickness (d_{Co}~1.2nm), showing that the Co film thinner than 1.2nm is not FM ordered at room temperature. Since bulk Co is always FM no matter it is in hcp, fcc, or bcc structural phase, the absence of the FM order for d_{Co}<1.2nm has to be due to either a lower Curie temperature (T_C) than the measurement temperature or a non-FM nature of the material. It is well known that the T_C value of a FM thin film increases with film thickness to approach its bulk value [34], thus it is possible that a FM film could loss its FM order at a given temperature below a critical thickness. Then the interesting question is if the absence of the hysteresis loop of Co/Bi_2Se_3 at d_{Co}<1.2nm is due to a reduced T_C or the non-FM nature of the material? To distinguish these two cases, we performed thickness-dependent study of the MOKE signal [Fig. 2(b)]. Since the MOKE signal is proportional to the FM thickness within the light penetration

depth [33], the MOKE signal of the Co film should increases linearly with film thickness at least up to ~10nm [35]. If the entire Co film is in FM state at thicker thickness, the linear extrapolation at zero MOKE signal should correspond to zero Co thickness. This procedure has been practiced routinely in magnetic ultrathin films such as Co/Cu [35] and Fe/Ag [36]. Then the interesting observation of Fig. 2(b) is that the linear extrapolation at zero Kerr signal gives $d_{Co}\approx$1.2nm for Co/Bi_2Se_3, showing that ~1.2nm Co is magnetically dead at the Co/Bi_2Se_3 interface rather than having a lower T_C.

We further performed thickness-dependent measurement of the Co/Bi_2Se_3 using element-specific X-ray Magnetic Circular Dichroism (XMCD) at the beamline 6.3.1 of the Advanced Light Source (ALS) of the Lawrence Berkeley National Laboratory. Wedge shaped Co film was grown by moving the substrate behind a knife-edge shutter during the Co film growth [32] so that the XMCD measurement at different positions of the sample provides a systematic thickness-dependent study. The film was covered by 2nm Ag to protect from contamination before taking it to the ALS. Circular polarized x-ray is delivered to the sample at 60^o incident angle, and X-ray Absorption Spectrum (XAS) at the Co 2p core level (L_2 and L_3 edges) is taken at T=80K within an external magnetic field. Then the XAS asymmetry at B=±5000 Oe, $XMCD \equiv \frac{I(+B)-I(-B)}{I(+B)+I(-B)}$, is proportional to the magnetization of the sample [37]. Because of the element specificity of the core level absorption, the XMCD measures only the Co magnetization rather than of the whole sample as in the MOKE measurement. Fig. 3(a) shows the XAS and XMCD at three different Co thicknesses. While XMCD is definitely present at d_{Co}=2.0 nm, we obtain no XMCD at d_{Co}=0.6 and 0.3 nm, showing the absence of FM order at d_{Co}=0.6 nm and 0.3 nm at T=80K. The XMCD signal increases linearly with the Co thickness but the linear extrapolation at zero XMCD signal gives d_{Co}=1.2 nm [Fig. 3(c)], in agreement with the MOKE measurement.

The MOKE and XMCD results show that ~1.2nm Co at the Co/Bi_2Se_3 interface is not FM ordered, suggesting an intermixing between Co and Bi_2Se_3 at the interface. It is well known that Co and Se form many different CoSe phases [38]. We find that the Co 2p peak itself below 1.2nm in Co/Bi_2Se_3 shows little difference from that of metallic Co, making it impossible to identify the CoSe phase simply from the Co 2p XAS [39]. Obviously other techniques are required to identify the Co/Bi_2Se_3 interfacial intermixing phase. Alternatively, we addressed this issue by growing a sample of Co/Ag(3nm)/Bi_2Se_3

with the 3nm Ag to isolate the intermixing between Co and Bi_2Se_3. It is well known that Co and Ag are immiscible and their equilibrium phase diagram shows no intermetallic compounds. The absence of the LEED pattern [Fig. 1(d)] from Ag(3nm)/Bi_2Se_3 shows that the 3nm Ag overlayer forms polycrystalline film and covers completely the Bi_2Se_3 substrate. XMCD measurement on Co/Ag(3nm)/Bi_2Se_3 was performed at T=80K. The result shows non-zero XMCD signal of Co film as thin as 0.3nm [Fig. 3(b)]. Moreover, a linear dependence of the XMCD signal on Co film thickness was observed with a linear extrapolation of d_{Co}=0 at zero XMCD signal, showing that the entire Co film in the Co/Ag(3nm)/Bi_2Se_3 is FM ordered [Fig. 3(c)]. To further prove that the loss of the FM order of the Co film at the Co/Bi_2Se_3 interface is due to the interfacial mixing, we grow another sample of Co/Ag(1nm)/Bi_2Se_3. Unlike the LEED result of 3nm Ag which shows a complete disappearance of the Bi_2Se_3(111) LEED diffraction spots, the weak LEED spots from the 1nm Ag on top of Bi_2Se_3(111) indicate that the 1 nm Ag layer does not fully cover the Bi_2Se_3 substrate [Fig. 1(c)]. Then the Co/Ag(1nm)/Bi_2Se_3 sample should allow certain degree of Co/Bi_2Se_3 intermixing. Indeed the XMCD result shows that the linear extrapolation at zero XMCD signal yields d_{Co}=0.8 nm, i.e., an equivalent of 0.8 nm Co is magnetically dead in Co/Ag(1nm)/Bi_2Se_3 [Fig 3(c)]. To further identify the existence of CoSe phase at the Co/Bi_2Se_3 interface, we notice that CoSe exhibits a very small shoulder just 3-5 eV above the Co L_3 edge although it is difficult to retrieve a quantitative intensity of this shoulder [40]. By comparing the XAS at different Co thicknesses and XAS of Co/Ag(3nm)/Bi_2Se_3, this shoulder is clearly present in the Co/Bi_2Se_3 sample at d_{Co}=0.2nm and 0.4nm (Fig. 4), supporting that CoSe phase is formed at the Co/Bi_2Se_3 interface. Since the should is quite weak and that XAS is a surface sensitive technique, it is very difficult to perform a quantitative analysis on the CoSe compounds. We leave it as an open question for future experiments to find a better way to characterize the CoSe intermixing phase at the Co/Bi_2Se_3 interface.

4. Summary

In summary, Co films grown on Bi_2Se_3 were studied using MOKE and XMCD. The result shows that ~1.2nm Co at the Co/Bi_2Se_3 interface is not FM ordered. By inserting 3nm Ag at the Co/Bi_2Se_3 interface, the Co film becomes completely FM ordered including the Co/Ag interface, showing that the loss of the FM order of the Co film at the Co/Bi_2Se_3 interface is due to the intermixing between Co and Bi_2Se_3. Since many

theoretical models assumed a magnetically ordered interface in FM/TI system, our result demands an examination of these models to take into account of the magnetic dead layer at the interface.

Acknowledgement

This work was supported by National Science Foundation DMR-1210167, U.S. Department of Energy DE-AC02-05CH11231, and NRF through Global Research Laboratory project of Korea.

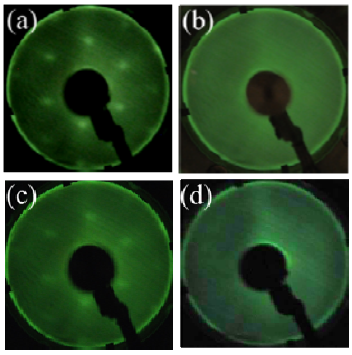

Fig. 1: (color online) LEED patterns of (a) Bi_2Se_3(111) substrate, (b) Co(2nm)/ Bi_2Se_3(111) , (c) Ag(1nm)/ Bi_2Se_3(111) , and (d) Ag(3nm)/ Bi_2Se_3(111) . The absence of LEED spots in (b) and (d) shows polycrystalline formation of 2nm Co and 3nm Ag films and a complete coverage of the films on Bi_2Se_3(111) substrate. The weak LEED spots in (c) show a partial coverage of the 1nm Ag on Bi_2Se_3.

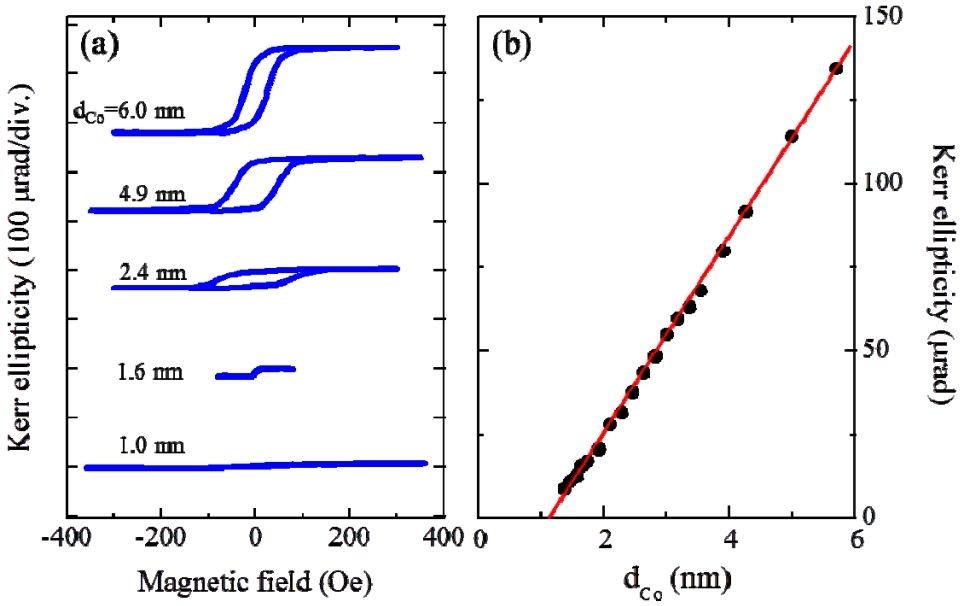

Fig. 2: (color online) (a) Hysteresis loops and (b) Kerr ellipticity of Co films on Bi_2Se_3 substrate from MOKE measurement. The 1.2nm Co intersection thickness at zero Kerr signal shows that there exists 1.2nm ferromagnetically dead layer in the Co film.

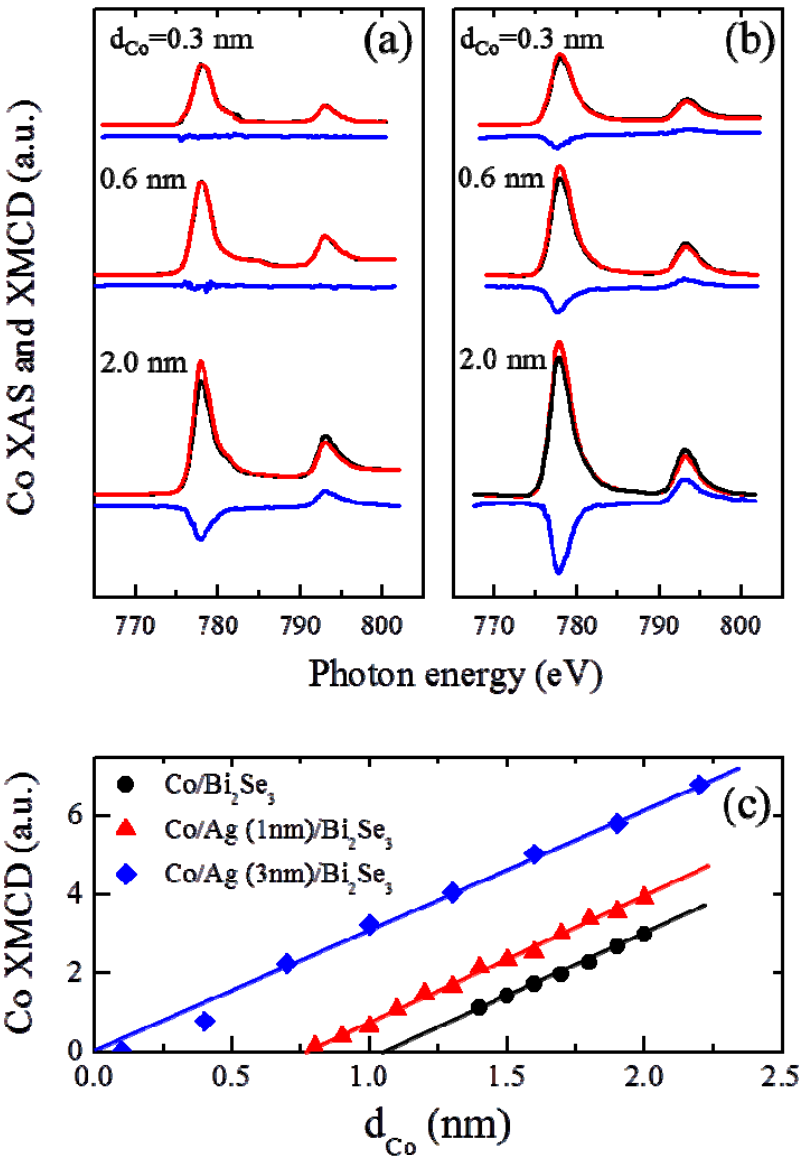

Fig. 3: (color online) Co XAS (black and red lines) and XMCD (blue lines) of (a) Co/Bi_2Se_3 and (b) $Co/Ag(3nm)/Bi_2Se_3$. Red and black lines are XAS at B=+5000 Oe and B=-5000 Oe, respectively. (c) XMCD signal vs Co thickness. The zero Co intersection thickness for $Co/Ag(3nm)/Bi_2Se_3$ shows a ferromagnetic ordering of the entire Co film, in contrast to the 0.8nm and 1.2nm magnetic dead layers in $Co/Ag(1nm)/Bi_2Se_3$ and Co/Bi_2Se_3, respectively.

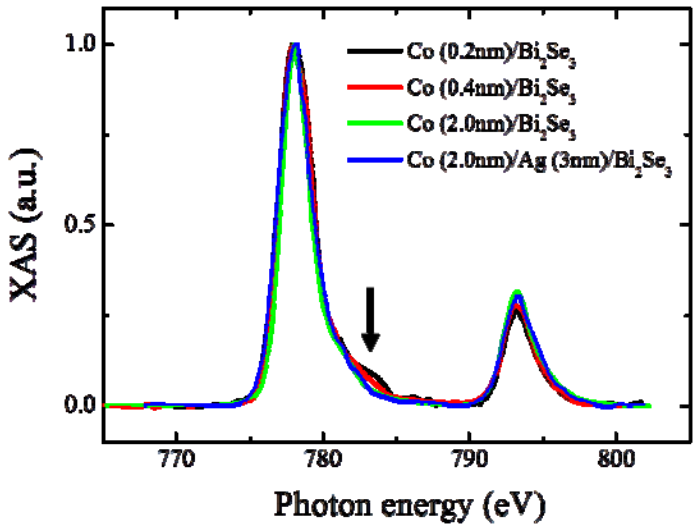

Fig. 4: (color online) XAS of the films as indicated in the figure. The small shoulder (shown by the arrow) is the evidence of CoSe formation at the Co/Bi_2Se_3 interface.

References:

1. C. L. Kane and E. J. Mele, Phys. Rev. Lett. **95**, 146802 (2005).
2. B. A. Bernevig, T. L. Hughes, and S. C. Zhang, Science **314**, 1757 (2006).
3. L. Fu, C. L. Kane, and E. J. Mele, Phys. Rev. Lett. **98**, 106803. (2007).
4. J. E. Moore, and L. Balents, Phys. Rev. B **75**, 121306(R) (2007).
5. R. Roy, Phys. Rev. B **79**, 195322 (2009).
6. M. König, S. Wiedmann, C. Brune, A. Roth, H. Buhmann, L.W. Molenkamp, X. L. Qi, and S. C. Zhang, Science **318**, 766 (2007).
7. D. Hsieh, D. Qian, L. Wray, Y. Xia, Y. S. Hor, R. J. Cava and M. Z. Hasan, Nature **452**, 970 (2008).
8. Joel E. Moore, Nature **464**, 194 (2010).
9. M. Z. Hasan and C. L. Kane, Rev. Mod. Phys. **82**, 3045 (2010).
10. Pedram Roushan, Jungpil Seo, Colin V. Parker, Y. S. Hor, D. Hsieh, Dong Qian, Anthony Richardella, M. Z. Hasan, R. J. Cava and Ali Yazdani, Nature **460**, 1106 (2009).
11. Zhanybek Alpichshev, J. G. Analytis, J.-H. Chu, I. R. Fisher, Y. L. Chen, Z. X. Shen, A. Fang, and A. Kapitulnik, Phys. Rev. Lett. **104**, 016401 (2010).
12. Qin Liu, Chao-Xing Liu, Cenke Xu, Xiao-Liang Qi, and Shou-Cheng Zhang, Phys. Rev. Lett. **102**, 155603 (2009).
13. Wang-Kong Tse and A. H. MacDonald, Phys. Rev. Lett. **105**, 057401 (2010)
14. R. Valde´s Aguilar, A.V. Stier, W. Liu, L. S. Bilbro, D. K. George, N. Bansal, L. Wu, J. Cerne, A. G. Markelz, S. Oh, and N. P. Armitage, Phys. Rev. Lett. **108**, 087403 (2012).
15. Hong-Tao He, Gan Wang, Tao Zhang, Iam-Keong Sou, George K. LWong, and Jian-Nong Wang Hai-Zhou Lu, Shun-Qing Shen, and Fu-Chun Zhang, Phys. Rev. Lett. **106**, 166805 (2011).
16. Minhao Liu, Jinsong Zhang, Cui-Zu Chang, Zuocheng Zhang, Xiao Feng, Kang Li, Ke He, Li-li Wang, Xi Chen, Xi Dai, Zhong Fang, Qi-Kun Xue, Xucun Ma, and Yayu Wang, Phys. Rev. Lett. **108**, 036805 (2012).
17. Y. L. Chen, J.-H. Chu, J. G. Analytis, Z. K. Liu, K. Igarashi, H.-H. Kuo, X. L. Qi, S. K. Mo, R. G. Moore, D. H. Lu, M. Hashimoto, T. Sasagawa, S. C. Zhang, I. R. Fisher, Z. Hussain, and Z. X. Shen, Science **329**, 659 (2010).
18. Yoshinori Okada, Chetan Dhital, Wenwen Zhou, Erik D. Huemiller, Hsin Lin, S. Basak, A. Bansil, Y.-B. Huang, H. Ding, Z. Wang, Stephen D. Wilson, and V. Madhavan, Phys. Rev. Lett. **106**, 206805 (2011).

19. Y. S. Hor, P. Roushan, H. Beidenkopf, J. Seo, D. Qu, J. G. Checkelsky, L. A. Wray, D. Hsieh, Y. Xia, S.-Y. Xu, D. Qian, M. Z. Hasan, N. P. Ong, A. Yazdani, and R. J. Cava, Phys. Rev. B **81**, 195203 (2010).

20. Ivana Vobornik, Unnikrishnan Manju, Jun Fujii, Francesco Borgatti, Piero Torelli, Damjan Krizmancic, Yew San Hor, Robert J. Cava, and Giancarlo Panaccione, Nano Lett. **11**, 4079 (2011).

21. L. AndrewWray, Su-Yang Xu, Yuqi Xia, David Hsieh, Alexei V. Fedorov, Yew San Hor, Robert J. Cava, Arun Bansil, Hsin Lin, and M. Zahid Hasan, Nature Physics **7**, 32, (2011).

22. T. Valla, Z.-H. Pan, D. Gardner, Y. S. Lee, and S. Chu, Phys. Rev. Lett. **108**, 117601 (2012).

23. D. West, Y. Y. Sun, B. Zhang, T. Zhang, Xucun Ma, P. Cheng, Y. Y. Zhang, X. Chen, J. F. Jia, and Q. K. Xue, Phys. Rev. B **85**, 081305(R) (2012).

24. J. Honolka, A. A. Khajetoorians, V. Sessi, T. O. Wehling, S. Stepanow, J.-L. Mi, B. B. Iversen, T. Schlenk, J. Wiebe, N. Brookes, A. I. Lichtenstein, Ph. Hofmann, K. Kern, and R. Wiesendanger, to be published.

25. M. Ye, S. V. Eremeev, K. Kuroda, E. E. Krasovskii, E. V. Chulkov, Y. Takeda, Y. Saitoh, K. Okamoto, S. Y. Zhu, K. Miyamoto, M. Arita, M. Nakatake, T. Okuda, Y. Ueda, K. Shimada, H. Namatame, M. Taniguchi, and A. Kimura, Phys. Rev. B **85**, 205317 (2012).

26. J. Henk, A. Ernst, S. V. Eremeev, E. V. Chulkov, I. V. Maznichenko, and I. Mertig, Phys. Rev. Lett. **108**, 206801 (2012).

27. Ion Garate and M. Franz, Phys. Rev. Lett. **104**, 146802 (2010).

28. Yaroslav Tserkovnyak and Daniel Loss, Phys. Rev. Lett. **108**, 187201 (2012).

29. D. A. Abanin and D. A. Pesin, Phys. Rev. Lett. **106**, 136802 (2011).

30. S. D. Bader and S. S. P. Parkin, Annual Review of Condensed Matter Physics **1**, 71 (2010).

31. S. Mondal, D. Sen, K. Sengupta, and R. Shankar, Phys. Rev. Lett. **104**, 046403 (2010).

32. Ernesto J. Escorcia-Aparicio, R. K. Kawakami, and Z. Q. Qiu, Phys. Rev. B **54**, 4155 (1996).

33. Z. Q. Qiu and S. D. Bader, Rev. of Sci. Inst. **71**, 1243 (2000).

34. Renjun Zhang and Roy F. Willis, Phys. Rev. Lett. **86**, 2665 (2001).

35. Z. Q. Qiu, J. Pearson, and S. D. Bader Phys. Rev. B **46**, 8195 (1992).

36. Z. Q. Qiu, J. Pearson, and S. D. Bader Phys. Rev. Lett. **67**, 1646 (1991).

37. J. Wu, J. S. Park, W. Kim, E. Arenholz, M. Liberati, A. Scholl, Y. Z. Wu, Chanyong Hwang, and Z. Q. Qiu, Phys. Rev. Lett. **104**, 217204 (2010).

38. A. Goswami and P. S. Nikam, J. of Crystal Growth **8**, 247 (1971).

39. A. B. Mandale, S. Badrinarayanan, S. K. Date, and A. P. B. Sinha, J. of Electron Spectroscopy and Related Phenomena **33**, 61 (1984).

40. J. M. Charnock, C. M. B. Henderson, J. F. W. Mosselmans, and R. A. D. Pattrick, Phys. Chem. Minerals **23**, 403 (1996).